PAPER • OPEN ACCESS

Effect of top cell absorber thickness and bifacial illumination on monolithic (Ag,Cu)(In,Ga)Se$_2$/Si tandem solar cells

To cite this article: Julia Horstmann *et al* 2025 *J. Phys. Energy* **7** 045004

View the article online for updates and enhancements.

You may also like

Journal of Physics: Energy

PAPER

OPEN ACCESS

Effect of top cell absorber thickness and bifacial illumination on monolithic (Ag,Cu)(In,Ga)Se$_2$/Si tandem solar cells

Julia Horstmann[1,*] [ID], Mario Hanser[2], Jana-Isabelle Polzin[2], Matthias Maiberg[1], Roland Scheer[1] [ID] and Martin Hermle[2]

1 Photovoltaics Group, Institute of Physics, Martin-Luther-University Halle-Wittenberg, Halle, Germany
2 Division Photovoltaics, Fraunhofer Institute for Solar Energy Systems ISE, Freiburg, Germany
* Author to whom any correspondence should be addressed.

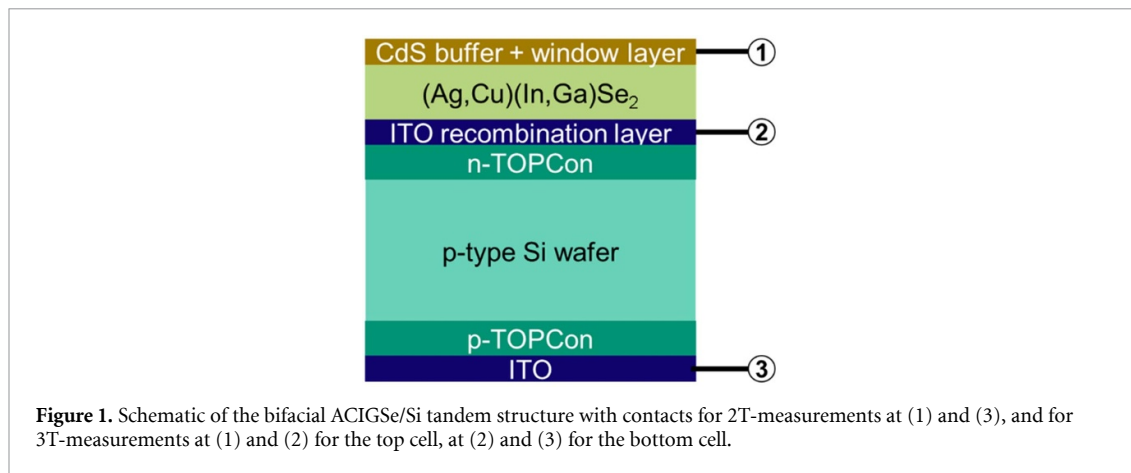E-mail: julia.horstmann@physik.uni-halle.de

Abstract

Wide bandgap (Ag,Cu)(In,Ga)Se$_2$ (ACIGSe) is a viable candidate as top cell absorber in tandem devices. In this work, we investigate monolithic two-terminal ACIGSe-Si tandem cells with a bandgap of 1.5 eV. Our research focuses on the direct preparation of the ACIGSe top cell on the Si bottom cell, the impact of the top cell absorber thickness and the gain through bifacial illumination. Bifacial monocrystalline silicon solar cells with tunnel oxide passivated contacts (TOPCon) are used as bottom cells. Considering that the TOPCon structure allows high temperature treatments without severe device degradation, TOPCon silicon cells are in principle suitable for ACIGSe deposition at evaporation temperatures of approximately 600 °C. Variation of the ACIGSe absorber thicknesses reveals an optimum for low top cell absorber thicknesses. The optimum shifts to thicker absorbers of 1 μm when operating the tandem device bifacially with back illumination reaching the highest output power of 16.2 mW cm^{-2} with addition rear illumination of 52% of 1-sun illumination. An electro-optical computer simulation supports the experimental outcome.

1. Introduction

The interest in tandem solar cells rises due to their potential to mitigate carrier thermalization losses thereby surpassing the single-junction Shockley–Queisser limit. Crystalline silicon (c-Si) is a suitable bottom cell material due to its low bandgap of 1.12 eV, combined with low cost, high reliability, and a well-established commercial fabrication process [1]. It is currently the subject of intensive research in combination with perovskite top cells, enabling power conversion efficiencies (PCE) of up to 34.9% [2, 3]. However, major challenges related to long-term stability and reliability persist, which complicates the widespread adoption of perovskite-based top cells [4].

As a stable alternative, wide bandgap ((Ag,)Cu)(In,Ga)Se$_2$ ((A)CIGSe) is a promising absorber material for the top cell. Narrow bandgap (~1.2 eV) ACIGSe solar cells have achieved efficiencies greater than 23% [5]. However for tandem structures, a top cell with a bandgap above 1.5 eV is required, for which ACIGSe solar cells have reached an efficiency of merely 14.8% in single-junction configurations [6, 7]. The first chalcopyrite/c-Si tandem, reaching an efficiency of 9.7%, was published by Jeong *et al* in and remained the highest published efficiency for this structure, far below its theoretical potential [8].

Wide bandgap CIGSe is readily obtained by increasing the Ga/In-ratio, but the material suffers from deep defect states [9–11], higher defect densities [12] and an unfavorable conduction band offset, leading to increased interface recombination [13, 14]. It has been shown, however, that these drawbacks can be compensated by partial substitution of Cu with Ag, whereby grain size is enhanced, structural disorder is reduced due to recrystallization [7, 15, 16], and interface recombination is reduced through lowering of the conduction band minimum [17].

Figure 1. Schematic of the bifacial ACIGSe/Si tandem structure with contacts for 2T-measurements at (1) and (3), and for 3T-measurements at (1) and (2) for the top cell, at (2) and (3) for the bottom cell.

This work is a conceptual study on monolithic grown 2-terminal (2T) tandem solar cells with ACIGSe as top and c-Si with tunnel oxide passivated contacts (TOPCon) as bottom cells using indium-doped tin oxide (ITO) as both the recombination layer (RL) and back contact of the Si sub-cell (figure 1). The TOPCon c-Si solar cells combine different advantages as bottom cells in tandem devices. First, high efficiencies of 26% for silicon single-junction solar cells [18] have been reached through such a carrier-selective passivating contact. Furthermore, the TOPCon structure enables high temperature processing without significant device degradation, making it suitable for ACIGSe deposition at evaporation temperatures around 600 °C [19].

The 2T configuration uses an internal junction to connect the sub-cells in series. That potentially reduces the costs for interconnections, as less material and less fabrications steps are needed. Further only two external contacts are required. In this configuration, the voltage of the tandem is the sum of both sub-cells, while the current is determined by the sub-cell with the lower photocurrent. The top cell must be transparent to photons with energies below its bandgap, allowing these photons to be absorbed by the bottom cell. The amount of light absorbed (and consequently the generated current) depends on the thickness and bandgap of the absorber. The optimum is reached when both sub-cells generate the same amount of current, a condition known as current matching.
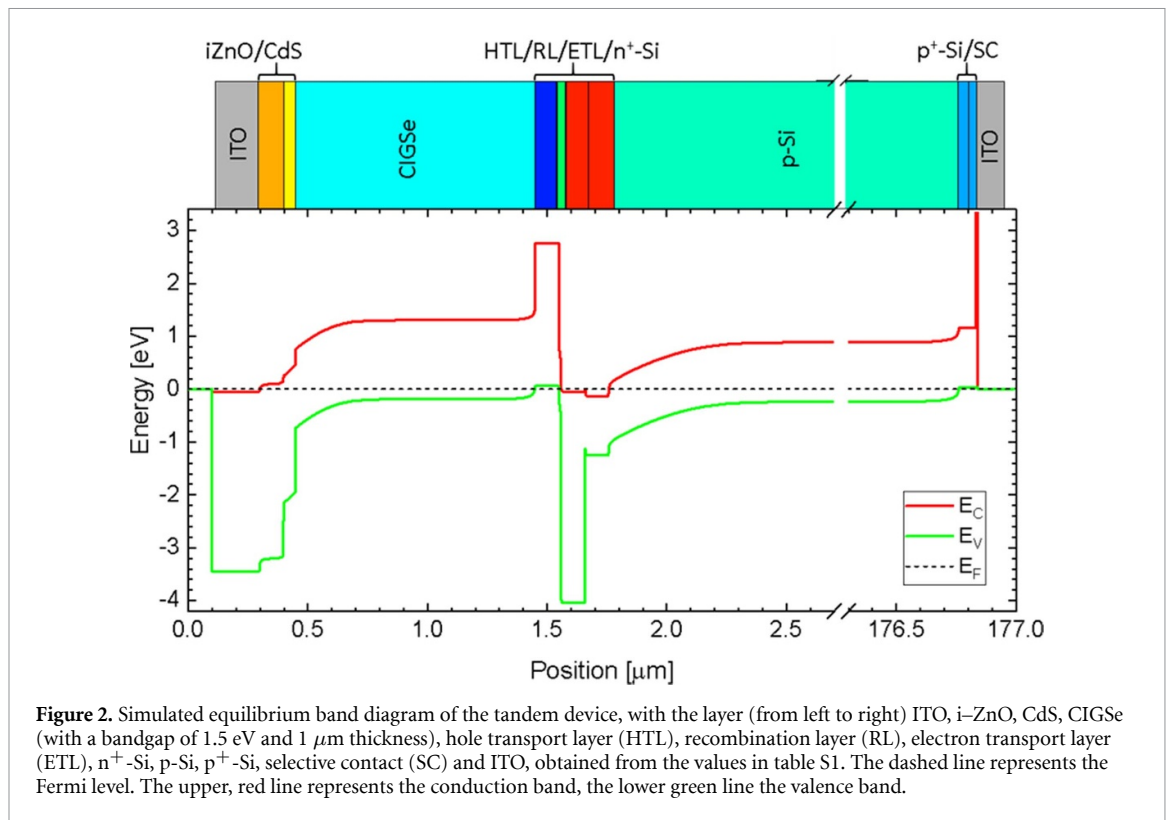
Previous simulations of the chalcopyrite/c-Si structure, with fixed values for the Si bottom cell, have shown that current matching occurs at a relatively large top cell bandgap around 1.65 eV. This bandgap allows current matching while maintaining realistic top cell absorber thicknesses above 0.2 μm [20]. As pointed out above, a large bandgap of ACIGSe can principally be realized by a high Ga content. However, such high Ga content above 90% (with respect to In) impedes a high efficiency of ACIGSe single-junction solar cells [21, 22].

Therefore, our approach aims to utilize an ACIGSe top cell with a bandgap of approximately 1.5 eV in the tandem structure, while compensating for the reduced current generation in the bottom cell with rear-side illumination via albedo reflection. This requires a bifacial bottom cell architecture, which is realized by using ITO as back contact on the p-type TOPCon. In this configuration, the optimization of the ACIGSe top cell is no longer constrained by the need to achieve higher bandgaps. In the present work, we investigate bifacial ACIGSe/Si tandem solar cells by varying the top cell absorber thickness and the intensity of rear-side illumination. Current-matching conditions and the highest output powers are identified through both experimental analysis and electro-optical computer simulations.

2. Experiment

2.1. Sample preparation
The tandem structure employed in the work is shown in figure 1. The bottom cell was prepared by Fraunhofer ISE using 5 Ωcm p-type Czochralski-grown wafer with a thickness of 175 μm. After saw-damage removal and standard cleaning, both sides were thermally oxidized to form an ultra-thin SiO$_x$. Phosphorus-or Boron doped amorphous Si was deposited by plasma-enhanced chemical vapor deposition (PECVD) on the front for n-type and on the rear side for p-type doping with a thickness of approximately 100 and 72 nm, respectively. The structure was then annealed at 925 °C for 10 min in nitrogen atmosphere and hydrogenated using a 70 nm hydrogen-rich PECVD SiN$_x$ layer followed by a 550 °C annealing for 10 min in nitrogen. The dielectric layer was removed before further processing. Both sides were coated with 50 nm ITO (enabling bifacial operation) and hot-plate annealed at 300 °C for 5 min to cure sputter damage.

Figure 2. Simulated equilibrium band diagram of the tandem device, with the layer (from left to right) ITO, i–ZnO, CdS, CIGSe (with a bandgap of 1.5 eV and 1 μm thickness), hole transport layer (HTL), recombination layer (RL), electron transport layer (ETL), n^+-Si, p-Si, p^+-Si, selective contact (SC) and ITO, obtained from the values in table S1. The dashed line represents the Fermi level. The upper, red line represents the conduction band, the lower green line the valence band.

The cells were laser-cut to 2.54×2.54 cm^2 and an Ag rear grid was applied (shading $\sim$12%–19% of active area, exemplary pictures of the tandem structures are shown in figure S2 in the SI).
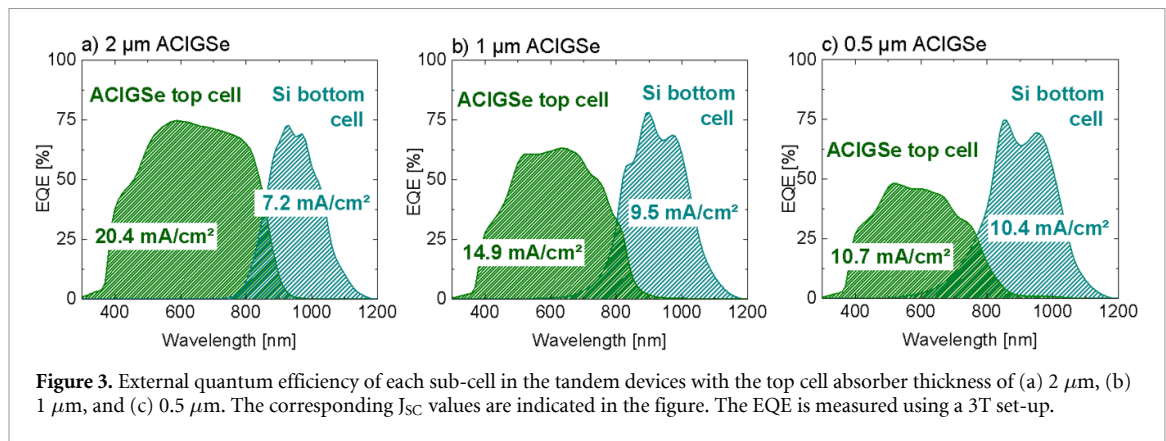
On top of the front ITO the ACIGSe top cell absorber was prepared in a modified 3-stage co-evaporation process at high substrates temperatures up to 600 °C. Ag was added during the first stage, together with In, Ga and Se. The targeted [Ag]/[Ag + Cu]-ratio is 0.07. In the second stage Cu, Ga, and Se were evaporated simultaneously. Adding Ga in the second stage removes a Ga notch formed through the low Ga diffusion, which causes electrical losses [23]. In the third stage In and Ga were added again at constant Se flux until the desired [Ag + Cu]/[Ga + In]-ratio of 0.8–0.9 is reached. The In and Ga fluxes are set to a [Ga]/[Ga + In]-ratio of 0.78–0.84. ACIGS film thickness of 0.5 μm, 1 μm, and 2 μm were realized by adjusting the process time. Approximately 30 nm NaF and RbF layers were deposited as post-deposition treatment at substrate temperatures of 450 °C. The top cell was finished with the CdS buffer by chemical bath deposition and sputtered iZnO/ITO window layer. The window and buffer layers are etched to 9 individual ACIGSe cells, with an active area of approximately 0.3–0.5 cm^2, as pictured in S2 in the SI.

2.2. Characterization

The tandem solar cell devices were characterized by current-density—voltage (JV) analysis under standard testing conditions at 25 °C using two WAVELABS Sinus70 sun simulators. Front illumination was provided from the top with 1-sun AM1.5 G spectrum. For bifacial measurements, the second simulator illuminated the back side through glass at 13, 30, and 100% of AM1.5 G equivalent. To prevent overheating of the solar cell in the absence of sample cooling, flash illumination was used. Masks with an area of 0.24 cm^2 define the illuminated area of both sub-cells in mono- and bifacial setups. JV measurements were performed at 2T configuration, contacting terminal (1) and (3) in figure 1. The solar cell data given below correspond to the champion cell of each batch.

External quantum efficiency (EQE) was measured from 300–1300 nm with 10 nm resolution with a Bentham PVE300 instrument, without bias light (dark EQE). A third terminal was added at the ITO RL to enable 3T-EQE measurements of each sub-cell. In figure 1 this corresponds to terminal (1) and (2) for the top cell and terminal (2) and (3) for the bottom cell.

The composition of the ACIGSe absorber was analyzed by glow discharge optical emission spectroscopy using a Spectruma GDA750 system. The ACIGSe layer thickness was determined from the cross-section by scanning electron microscopy using a SUPRA 40VP from Zeiss.

Figure 3. External quantum efficiency of each sub-cell in the tandem devices with the top cell absorber thickness of (a) 2 μm, (b) 1 μm, and (c) 0.5 μm. The corresponding J_{SC} values are indicated in the figure. The EQE is measured using a 3T set-up.

2.3. Simulation

Synopsys TCAD software was used to build an electro-optical computer model of the tandem structure. The series connection was established by a stack of electron transport layer (ETL), RL, and hole transport layer (HTL). For the silicon bottom cell, standard values for charge carrier mobility and the electrically active doping densities, provided by Fraunhofer ISE, were applied, while the charge carrier lifetime was adjusted to match the experimental solar cell parameters, resulting in an efficiency of approximately 21.4%, based on the average performance of the single-junction reference cell. For the ACIGSe top cell, there is no consistent simulation model available, so material parameters from Maiberg *et al* [24] for low bandgap CIGSe were adopted, with reduced minority carrier lifetimes. The recombination velocity at the ACIGSe/CdS interface is set to $S = 10^5$ cm s^{-1}. The selective contact (SC) between p$^+-$Si and ITO is highly n-doped to realize an ohmic contact. The front and back ITO layers are simulated as transparent metals. Material parameters are summarized in table S1, and the equilibrium energy band diagram is shown in figure 2.

To optimize output power, the top cell absorber thickness and the rear-side illumination have been varied. Ideal antireflection was assumed at both front and back surfaces. Illumination was applied with AM1.5 G spectrum from the top at an intensity of 0.1 W cm^{-2} and from the back with varying intensities from 0%– to 100%.

3. Results and discussion

The ACIGSe thickness was varied between 0.5 μm, 1 μm, and 2 μm, to understand the trade-off between light absorption in the top cell and the amount of light transmitted to the bottom cell. To systematically investigate the impact of absorber thickness, we first consider devices without back illumination.

3.1. EQE analysis

Using a 3T set-up, the EQE of each sub-cell was analyzed, as shown in figure 3. The EQE curves highlight the impact of increasing the top cell absorber thickness on the Si bottom cell. The 2 μm top cell absorber, which represents the standard thickness for ACIGSe single-junction solar cells, exhibits a significant mismatch between the sub-cells, as shown by the EQE graphs in figure 3(a). Considering the bandgap of 1.5 eV, only a limited amount of light is transmitted to the Si bottom cell. Reducing the top cell thickness to 1 μm (figure 3(b)) and 0.5 μm (figure 3(c)) decreases the absorption in the top cell. However, even with the thinnest absorber, the calculated current density of the bottom cell remains slightly below that of the top cell, indicating that the Si sub-cell is limiting the short-circuit current density of the tandem solar cell ($J_{SC,T}$). As predicted by simulation, achieving higher current generation in the bottom cell would require a wider bandgap in the top cell.

The EQE spectra of the ACIGSe sub-cells reach a maximum of only 75%, which can be attributed to absorption losses within a non-optimized window layer and high interface recombination at the ACIGSe/CdS interface [17]. The latter is supported by voltage-biased EQE measurements, presented in figure S3 in the SI. A drop in EQE across all wavelengths is observed under applied forward bias. The interference patterns visible in the EQE of the Si sub-cells originate from light reflected at the back contact of the ACIGSe top cell. As expected, the interference maxima become more closely spaced on the wavelength scale with increasing ACIGSe film thickness.
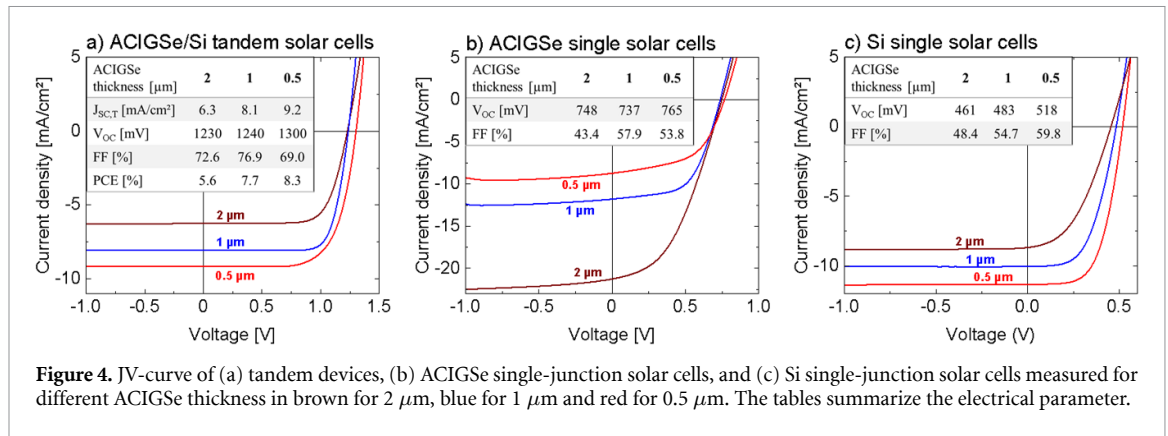
Figure 4. JV-curve of (a) tandem devices, (b) ACIGSe single-junction solar cells, and (c) Si single-junction solar cells measured for different ACIGSe thickness in brown for 2 μm, blue for 1 μm and red for 0.5 μm. The tables summarize the electrical parameter.

3.2. JV characterization

Figure 4(a) shows the illuminated JV-curves and electrical parameters of the 3Tandem devices with different absorber thicknesses. The JV was measured in the 2T set-up. The trend in $J_{SC,T}$ follows the EQE data with a monotonous increase in short-circuit current upon decreasing ACIGSe thickness. The slight difference between the $J_{SC,T}$ measured by EQE- and by JV-measurements originates from masking-errors in the JV set-up. Additionally, dark-EQE measurements do not account for the device's dependence on illumination conditions. The highest PCE of 8.3% reaches the tandem device with 0.5 μm top cell absorber thickness. At this point, the photocurrents generated in both sub-cells are nearly matched, also visible in the EQE measurement shown in figure 3(c). This current matching minimizes recombination losses that typically arise from photocurrent mismatch.

The measured open-circuit voltage (V_{OC}) of the tandem devices for all samples is lower than the expected value obtained by adding up the V_{OC} of both sub-cells. The loss results from the sample preparation and measurement setup. As described in section 2.1, the ACIGSe sub-cells are etched to an area of approximately 0.5 cm^{2}To minimize the risk of shunts, whereas the Si sub-cell retains its full area of 6.45 cm^2. To ensure that both sub-cells are illuminated over the same area, a mask with an area of 0.24 cm^2 is applied during the measurements. Consequently, the illuminated area of the Si bottom cell is significantly smaller than its total area. The resulting deviation in area for the photocurrent density and for the saturation current density reduces the V_{OC}. To mitigate this issue, alternative sample preparation techniques are being investigated in the future to ensure that both sub-cells have comparable active areas, thereby improving the accuracy of tandem device performance evaluation.

When analyzing the JV-curves of the tandem devices, it is difficult to differentiate the contribution of the top and bottom cell. To gain a deeper insight into the performance of the different top cell absorbers, measurements are conducted using the 3T configuration, with the ITO RL serving as the back contact. The JV-curves of the ACIGSe single-junction cells and the Si single-junction cells are shown in figures 4(b) and (c), respectively. Overall the fill factor (FF) in the single-junction measurements is low, since the 50 nm ITO layer, serving as back contact for the top cell, offers insufficient lateral conduction. As for the tandem device, the FF of the 0.5 μm and 2 μm ACIGSe single-junction cell is below the FF of the 1 μm sample. The ACIGSe deposition process was optimized for producing 1 μm absorber samples regarding the [Ag]/[Ag + Cu]-ratio and Alkali-PDT. Optimized deposition parameters for 1 μm absorber were not adjusted to thinner or thicker absorber layers. For example, the amount of NaF needed for grain boundary passivation could be higher for thicker absorber layers. For the single-junction Si sub-cells, the JV curves exhibit a low V_{OC}, which is attributed to the previously discussed area difference between the photocurrent density and saturation current density. With increasing ACIGSe thickness the V_{OC} gradually decreases, because the light intensity transmitted to the bottom cell is reduced. The V_{OC} of the tandem solar cell corresponds to the sum of the individual sub-cell voltages. However, the experimentally obtained V_{OC} of the tandem measured in 2T configuration is slightly above the sum of the single-junction voltages, which indicates a limitation of the 3T configuration.

3.3. Simulation of bifacial tandem operation

Reducing the thickness of the top cell absorber decreases its current generation, as shown in figure 4(b), while increasing the current generation in the bottom cell. Although this leads to current matching between the sub-cells, the $J_{SC,T}$ remains too low for efficient tandem solar cell operation. An alternative approach to achieve current matching, even for thicker top cell absorber and a bandgap of 1.5 eV, is additional back
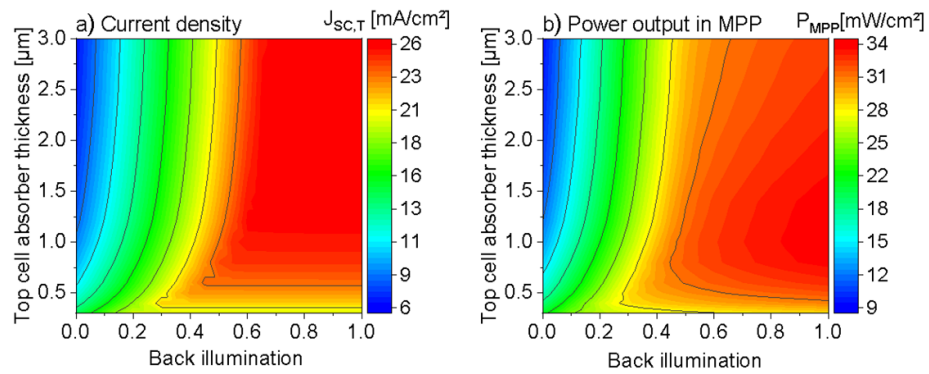
Figure 5. Simulated (a) current density and (b) output power in MPP for top cell absorber thickness from 0.3 to 3 μm and back illumination from 0 to 100%.

illumination. With this, both sub-cells generate more current. The bottom cell through back illumination and the top cell through increased thickness.

In the field, illumination entering from the backside can originate from reflected light from the ground beneath the solar module. The albedo, which describes the reflectivity of the ground, depends on its properties and is spectrally different. For example, the effective (spectral independent) albedo of green grass and white sand is approximately 24% and 67%, respectively [25]. In the experiments, as back illumination an effective albedo of 13% and 30% was used. The value of 13% represents lowly reflecting surfaces, while the 30% value is used as the average albedo. 100% albedo corresponds to 1-sun rear illumination with an intensity of 0.1 W cm^{-2}. A more realistic approach would account for the spectral dependence of each albedo, but this is beyond the scope of this investigation.

Opto-electronic simulations are used to understand the impact of top cell absorber thickness ($E_G = 1.5$ eV) under varying back illumination conditions. Figure 5 presents the resulting $J_{SC,T}$ and output power density at maximum power point (P_{MPP}). Corresponding FF and V_{OC} color plots are given in the SI in figure S1. Without back illumination, the highest $J_{SC,T}$ is achieved for ultrathin top cell absorber layers below 0.5 μm thickness. As the top cell thickness increases, the $J_{SC,T}$ decreases due to reduced light transmission to the current-limiting Si sub-cell. A minimum of 6 mA cm^{-2} reaches the Si sub-cell even for thick top cell absorbers. With increasing back illumination, the $J_{SC,T}$ rises for all thicknesses, though thicker top cell absorbers require a higher albedo to reach their maximum potential. For a 0.5 μm absorber, the current increases with up to 40% albedo, after which it saturates, indicating that the ultrathin ACIGSe sub-cell limits the current to approximately 22.6 mA cm^{-2}. In contrast, thicker ACIGSe layers can absorb more light, resulting in a maximum current of approximately 25 mA cm^{-2} for a 1 μm absorber with 57% albedo. These simulations highlight the effectiveness of back illumination in maximizing current generation in tandem devices.

The P_{MPP}, presented in figure 5(b), generally follows the trend of the $J_{SC,T}$, except for increased top cell thickness and high albedos. Recombination within the ACIGSe absorber leads to a reduced V_{OC}, this becomes more pronounced with increasing volume, as observed in thicker absorbers. This loss in V_{OC} consequently lowers the output power.

3.4. Experimental JV results under bifacial illumination

Experimentally, with the addition of back illumination, the $J_{SC,T}$ of the tandem device shifts towards the J_{SC} of the ACIGSe sub-cell ($J_{SC,TOP}$), taken from figure 4(b). This trend is evident for 1 and 2 μm ACIGSe absorber thicknesses, as shown in figure 6, where a consistent increase in $J_{SC,T}$ up to the point of current matching is observed. The increase in $J_{SC,T}$ for the 0.5 μm sample results cannot be explained by approaching the current matching, since from figure 3(c) it is obvious that the top cell should already limit the current to 10.7 mA cm^{-2}. This increase in current of 0.5 μm sample is rather attributed to a high shunt conductance of the top cell, a phenomenon discussed in detail later.

For 1 and 2 μm ACIGSe, the back illumination adds photons in the Si bottom cell, therefore increasing the $J_{SC,T}$ of the whole tandem, which was formerly limited by the bottom cell. That occurs until the current generated by the bottom cell reaches the current generated by the top cell. This limit is reached for the 1 μm cells with 30% albedo at 13.5 mA cm^{-2}. To analyze the theoretical maximum, also 100% back illumination was considered. No further increase in $J_{SC,T}$ is measured for 1 μm ACIGSe thickness. In contrast, the top cell limitation of 2 μm ACIGSe is reached between 30% and 100%. The V_{OC} of the tandem devices is not affected by the back illumination.
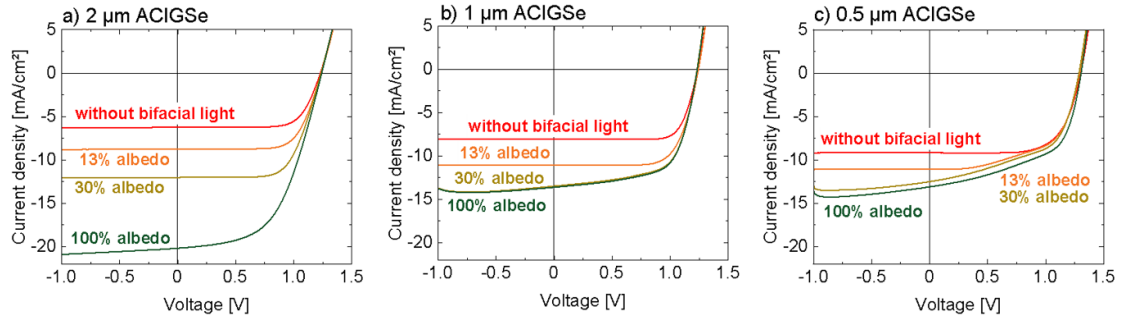
Figure 6. JV-curves without (red) and with increasing back illumination (13% in orange, 30% in yellow and 100% in green) for (a) 2 μm, (b) 1 μm, and (c) 0.5 μm top cell absorber thickness.
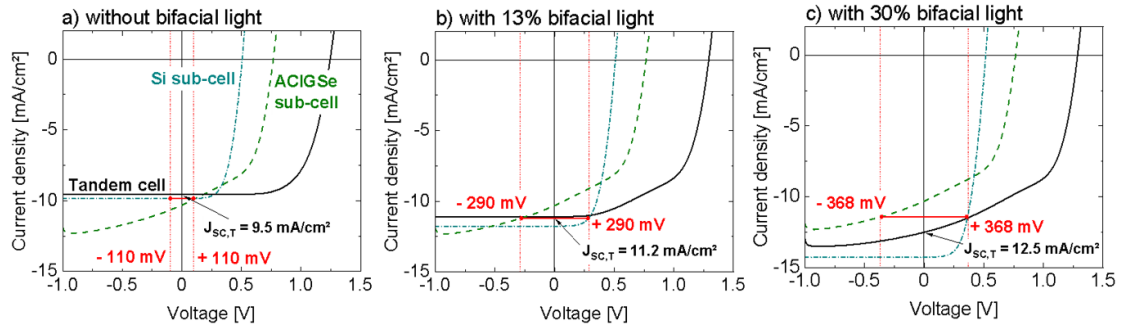

Figure 7. JV-characteristics for the tandem device with 0.5 μm absorber thickness (solid, black) (a) without back illumination, (b) with 13%, and (c) with 30% back illumination. Additional 3T-JV measurements of ACIGSe (green) and Si (blue) sub-cells demonstrate the impact of each sub-cell on $J_{SC,T}$. The red bar marks the theoretical position of $J_{SC,T}$.

3.5. Impact of shunt paths on $J_{SC,T}$ in the tandem solar cells

From the EQE in figure 3(c), the $J_{SC,T}$ for 0.5 μm ACIGSe thickness should increase from 10.4 to 10.7 mA cm^{-2} by albedo illumination. In contrast, the $J_{SC,T}$ is increased up to 13.1 mA cm^{-2}. Figure 7 illustrates the effect of the top cell's shunt conductance on the gain in $J_{SC,T}$, as determined by 3T-JV measurements. The sub-cells were measured individually under front and different back illumination intensities (0, 13 and 30%) to analyze each performance separately. Since the light from back illumination does not pass through the bottom cell to reach the top cell, no change in top cell current is observed. Without back illumination shown in figure 7(a), the Si sub-cell limits the current of the tandem device at approximately 9.5 mA cm^{-2}. (The $J_{SC,T}$ is slightly above the J_{SC} of the Si sub-cell ($J_{SC,Bottom}$), which results from slightly different masking between 3T and 2T measurements.) With 13% back illumination, the current generation in the bottom cell exceeds the $J_{SC,Top}$, see figure 7(b). In this case, the top cell should limit the current to 10.3 mA cm^{-2}. However, the $J_{SC,T}$ is 11.2 mA cm^{-2}.
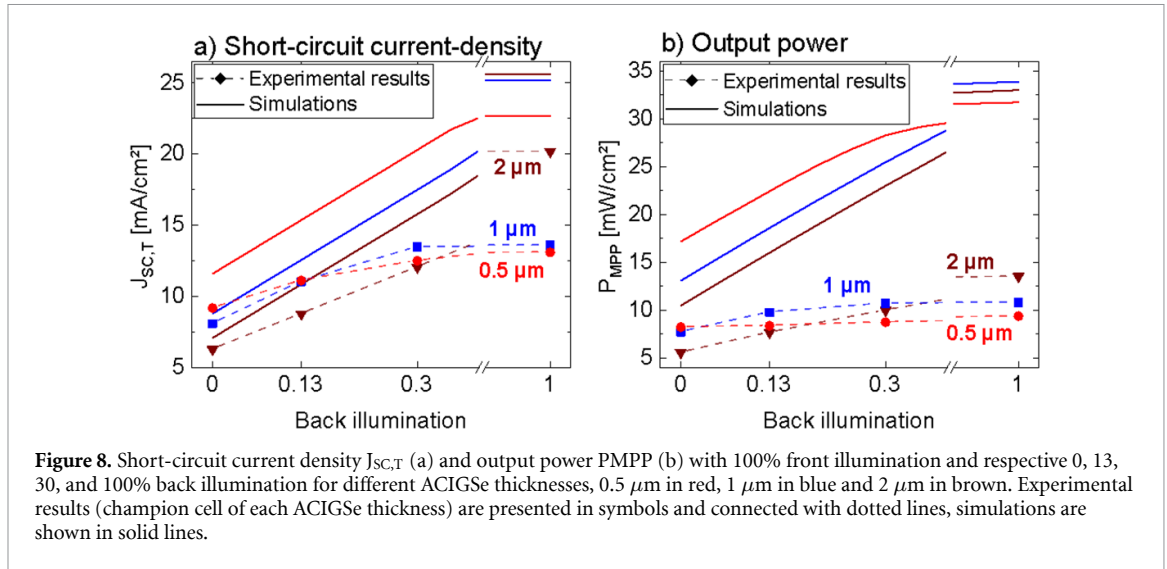
This phenomenon can be explained by Kirchhoff's laws, considering the sub-cells in a monolithic tandem solar cell are connected in series. The $J_{SC,T}$ of the tandem solar cell is defined from the following equations:

$$U_{SC,T} = U_{SC,Top} + U_{SC,Bottom} = 0 \tag{1}$$

$$J_{SC,T} = J_T(0V) = J_{Top}(U_{SC,Top}) = J_{Bottom}(U_{SC,Bottom}) \tag{2}$$

where $U_{SC,T}$ is the voltage of the tandem in short-circuit, $U_{SC,Top}$ and $U_{SC,Bottom}$ are the voltages of the ACIGSe and Si sub-cells, respectively. J is the current-density of the tandem (J_T), and of the ACIGSe (J_{Top}) and Si (J_{Bottom}) sub-cells. Equation (1) states that while the voltage across the complete tandem cell is zero, there may be partial voltages of opposite sign on the sub-cells. Equation (2) reflects the current-matching condition intrinsic to series-connected tandem devices.

To satisfy equation (1) under 13% albedo illumination, the sum of the voltages of the two sub-cells must be equal to zero. This is fulfilled when the ACIGSe top cell operates at –290 mV and the Si bottom cell at +290 mV. Due to the high shunt conductance of the top cell, the current densities at the operating points, $J_{Top}(-290\,\text{mV})$ and $J_{Bottom}(+290\,\text{mV})$, are equal, thereby fulfilling the equation (2). At this point, the $J_{SC,T}$ is no longer limited by the sub-cell with lower current generation but by $J_{Top}(-290\,\text{mV})$ which is larger than

Figure 8. Short-circuit current density $J_{SC,T}$ (a) and output power PMPP (b) with 100% front illumination and respective 0, 13, 30, and 100% back illumination for different ACIGSe thicknesses, 0.5 μm in red, 1 μm in blue and 2 μm in brown. Experimental results (champion cell of each ACIGSe thickness) are presented in symbols and connected with dotted lines, simulations are shown in solid lines.

the $J_{SC,TOP}$ due to shunt conductance of the top cell. The effect becomes more pronounced under 30% back illumination, since an even higher voltage is applied to the top cell. (Note that the deviation between $J_{SC,T}$ of 12.5 mA cm^{-2} and J_{Top}(−368 mV) of 11.5 mA cm^{-2} is attributed to measurement uncertainties between the 2T and 3T measurement set-up.) Without back illumination, the $J_{SC,T}$ is limited by the Si sub-cell, as mentioned above. At $J_{SC,T}$, the operating points of the sub-cells are J_{Top}(+110 mV) and J_{Bottom}(−110 mV). In contrast to the back illuminated results, the $J_{SC,T}$ is not visibly increased, as the shunt conductance of the Si sub-cell is very low.
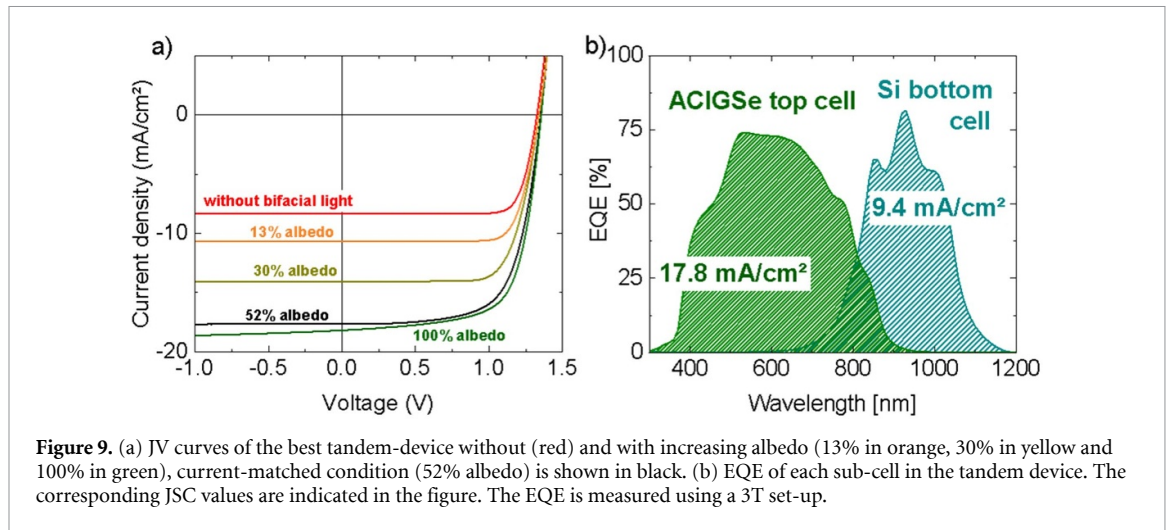
To summarize, increased rear illumination leads to higher current generation in the bottom cell, which elevates the operating bias of the individual sub-cells. Due to the high shunt conductance of the top cell, the $J_{SC,T}$ is greater than the J_{SC} of either individual sub-cell. The effect is also revealed by the slope of the JV curve. In low forward bias and negative bias regimes, the shunt conductance of the current limiting sub-cell is reflected in the tandem JV curve.

3.6. Comparison between experimental results and simulations

Figure 8 presents the electrical parameters, $J_{SC,T}$ (a) and P_{MPP} (b), as a function of top cell absorber thickness and back illumination intensity in experimental results and simulation. In the simulation without back illumination, the 0.5 μm sample achieves the highest $J_{SC,T}$, followed by the 1 μm and 2 μm samples. As back illumination increases, the current contribution from the bottom cell becomes apparent. The top cell eventually limits the current at 0.4 additional back side illumination for the 0.5 μm absorber, 0.6 for 1 μm, and 0.65 for 2 μm. The slightly higher current generation of the 2 μm sample compared to 1 μm is attributed to reduced back surface recombination in the thicker ACIGSe absorbers, as incorporated into the simulation.

The experimental results align with the simulation trends, except for the current gain in the 0.5 μm sample, which is lower in the experiment. The current of the 0.5 μm is already limited by the top cell with small albedo illumination, the slight increase in current is only due to the presence of shunt conductance in the 0.5 μm sample, as previously described. In the simulation, the current generation in the top cell is higher compared to the experimentally achieved values. Additionally, the experimental difference between the 1 μm and 2 μm samples at 100% albedo is more pronounced, as it correlates to the current generation in the ACIGSe sub-cell. For 1 μm ACIGSe thicknesses, losses are mostly in the near-infrared wavelength. This is also observable in the EQE spectra of the top cells (see figure 3). The losses may result from a reduced absorbance of low-energy photons and from back surface recombination, which has a stronger influence for thinner absorbers [26]. Simulations expect complete absorption above 1 μm ACIGSe absorber thickness.

Regarding the output power, the simulation results generally follow the trend of current density, except at high back illumination. In this regime, despite 1 μm and 2 μm having similar $J_{SC,T}$, the sample with 1 μm top cell absorber exhibits higher V_{OC} and FF, see figure S1 in SI. In the experimental data, however, the increase in $J_{SC,T}$ observed for the 0.5 μm sample does not translate into a proportional gain in the P_{MPP}. This discrepancy is primarily attributed to a significant reduction in FF, caused by high shunt conductance, which becomes increasingly pronounced under increasing back illumination. As a result, even at 100% back illumination, the gain in P_{MPP} is limited to only 1.15 mW cm^{-2} compared to no back illumination.

Figure 9. (a) JV curves of the best tandem-device without (red) and with increasing albedo (13% in orange, 30% in yellow and 100% in green), current-matched condition (52% albedo) is shown in black. (b) EQE of each sub-cell in the tandem device. The corresponding JSC values are indicated in the figure. The EQE is measured using a 3T set-up.

3.7. Record ACIGSe/Si device

Further optimization of the 1 μm ACIGSe top cell was conducted by adjusting the three-stage process. To prevent surface Ag accumulation, as reported in Prathapani *et al* [27], the Cu-rich phase during the second stage was minimized. As a result, we present a tandem structure achieving an output power density of 16.2 mW cm^{-2} with 52% albedo at current-matched condition. Figure 9 shows the JV curves under front illumination as well as under increasing back illumination (a) and the corresponding EQE-measurements of both sub-cells in the 3T-set-up (b). Given an input power of $P_{\mathrm{in}} = 152$ mW cm^{-2}, this corresponds to a PCE of 10.7%. However, in bifacial solar cells, where back illumination represents additional light that would otherwise be lost, evaluating performance based on P_{MPP} is more relevant than PCE. With a more realistic albedo of 30%, the P_{MPP} reaches 14.1 mW cm^{-2} (PCE = 10.8%). With the P_{MPP} increasing by over 50% relative to operation without back illumination ($P_{\mathrm{MPP}} = 8.9$ mW cm^{-2}), the results demonstrate the potential of bifacial ACIGSe/Si tandem solar cells. The current record for chalcopyrite/Si tandem solar cells, reported by Jeong *et al* at 9.7% [8], could be surpassed through targeted top cell optimization and the use of bifacial illumination to enhance photocurrent generation. However, it remains below the performance of perovskite/Si tandem solar cells, which have reached efficiencies up to 34.9% [3], despite ongoing challenges with long-term stability. The limited performance of ACIGSe top cells is primarily due to high interface recombination and low bulk carrier lifetimes, highlighting the need for further optimization to establish ACIGSe as an efficient top cell absorber material.

4. Conclusion

In this work, bifacial, monolithic 2T ACIGSe-Si tandem solar cells with different top cell absorber thicknesses are presented. The thickness is varied between the standard ACIGSe thicknesses of 2 μm down to an ultra-thin thickness of 0.5 μm. With the fixed bandgap of 1.5 eV, the Si bottom cell limits the current of the tandem device for all thicknesses. The highest current for monofacial tandem solar cells without albedo illumination is reached for 0.5 μm ACIGSe based tandem solar cells. But at this small thickness of ACIGSe, the low current generation in the top cell is limiting the efficiency of the tandem device. Therefore another approach to increase the $J_{\mathrm{SC,T}}$ is including albedo illumination from the rear side through the transparent back contact of the Si sub-cell. The highest output power of 16.2 mW cm^{-2} of a current-matched tandem solar cell is reached with 1 μm ACIGSe thickness and 52% albedo illumination. The $J_{\mathrm{SC,T}}$ of the tandem device with lower thicknesses, here 0.5 μm, also benefits from the albedo illumination, but only due to its high shunt conductance. The performance of wide-bandgap ACIGSe must be further optimized to enable its effective integration with Si in tandem devices. Back illumination provides a promising strategy to utilize thicker top cell absorbers, which demonstrate superior performance compared to ultrathin absorbers.

Data availability statement

All data that support the findings of this study are included within the article (and any supplementary files).

Acknowledgments

References

[1] Lu S, Chen C and Tang J 2020 Possible top cells for next-generation Si-based tandem solar cells *Front. Optoelectron.* **13** 246–55

[2] NREL Interactive best research-cell efficiency chart (available at: www.nrel.gov/pv/interactive-cell-efficiency) (Accessed 16 May 2025)

[3] pv-magazine 2025 LONGi achieves 34.85% efficiency for two-terminal tandem perovskite solar cell (available at: https://www.pv-magazine.com/2025/04/18/longi-achieves-34-85-efficiency-for-two-terminal-tandem-perovskite-solar-cell/) (Accessed 16 May 2025)

[4] Aydin E, Allen T G, de Bastiani M, Razzaq A, Xu L, Ugur E, Liu J and de Wolf S 2024 Pathways toward commercial perovskite/silicon tandem photovoltaics *Science* **383** eadh3849

[5] Keller J, Kiselman K, Donzel-Gargand O, Martin N M, Babucci M, Lundberg O, Wallin E, Stolt L and Edoff M 2024 High-concentration silver alloying and steep back-contact gallium grading enabling copper indium gallium selenide solar cell with 23.6% efficiency *Nat. Energy* **9** 467–78

[6] Keller J, Stolt L, Donzel-Gargand O, Violas A F, Kubart T and Edoff M 2024 Bifacial wide-gap (Ag,Cu)(In,Ga)Se$_2$ solar cell with 13.6% efficiency using In$_2$O$_3$:W as a back contact material *Sol. RRL* **8** 2400430

[7] Kim K *et al* 2018 Highly efficient Ag-alloyed Cu(In,Ga)Se$_2$ solar cells with wide bandgaps and their application to chalcopyrite-based tandem solar cells *Nano Energy* **48** 345–52

[8] Jeong A R, Choi S B, Kim W M, Park J-K, Choi J, Kim I and Jeong J-H 2017 Electrical analysis of c-Si/CGSe monolithic tandem solar cells by using a cell-selective light absorption scheme *Sci. Rep.* **7** 15723

[9] Eisenbarth T, Unold T, Caballero R, Kaufmann C A, Abou-Ras D and Schock H-W 2009 Origin of defects in CuIn$_{1-x}$Ga$_x$Se$_2$ solar cells with varied Ga content *Thin Solid Films* **517** 2244–7

[10] Huang B, Chen S, Deng H-X, Wang L-W, Contreras M A, Noufi R and Wei S-H 2014 Origin of reduced efficiency in Cu(In,Ga)Se$_2$ solar cells with high ga concentration: alloy solubility versus intrinsic defects *IEEE J. Photovolt.* **4** 477–82

[11] Spindler C, Babbe F, Wolter M H, Ehré F, Santhosh K, Hilgert P, Werner F and Siebentritt S 2019 Electronic defects in Cu(In,Ga)Se$_2$ towards a comprehensive model *Phys. Rev. Mater.* **3** 090302

[12] Hanna G, Jasenek A, Rau U and Schock H W 2001 Influence of the Ga-content on the bulk defect densities of Cu(In,Ga)Se$_2$ *Thin Solid Films* **387** 71–73

[13] Gloeckler M and Sites J R 2005 Efficiency limitations for wide-band-gap chalcopyrite solar cells *Thin Solid Films* **480–481** 241–5

[14] Li J V, Grover S, Contreras M A, Ramanathan K, Kuciauskas D and Noufi R 2014 A recombination analysis of Cu(In,Ga)Se$_2$ solar cells with low and high Ga compositions *Sol. Energy Mater. Sol. Cells* **124** 143–9

[15] Erslev P, Hanket G M, Shafarman W N and Cohen D J 2009 Characterizing the effects of silver alloying in chalcopyrite CIGS with junction capacitance methods *MRS Proc.* **1165** 1165–M01

[16] Hwang J *et al* 2021 Improved carrier transport in CIGS solar cells induced by Ag treatment *J. Alloys Compd.* **886** 161193

[17] Keller J, Sopiha K V, Stolt O, Stolt L, Persson C, Scragg J J, Törndahl T and Edoff M 2020 Wide-gap (Ag,Cu)(In,Ga)Se$_2$ solar cells with different buffer materials—A path to a better heterojunction *Prog. Photovolt., Res. Appl.* **28** 237–50

[18] Richter A, Müller R, Benick J, Feldmann F, Steinhauser B, Reichel C, Fell A, Bivour M, Hermle M and Glunz S W 2021 Design rules for high-efficiency both-sides-contacted silicon solar cells with balanced charge carrier transport and recombination losses *Nat. Energy* **6** 429–38

[19] Feldmann F, Bivour M, Reichel C, Hermle M and Glunz S W 2014 Passivated rear contacts for high-efficiency n-type Si solar cells providing high interface passivation quality and excellent transport characteristics *Sol. Energy Mater. Sol. Cells* **120** 270–4

[20] Kim K, Gwak J, Ahn S K, Eo Y-J, Park J H, Cho J-S, Kang M G, Song H-E and Yun J H 2017 Simulations of chalcopyrite/c-Si tandem cells using SCAPS-1D *Sol. Energy* **145** 52–58

[21] Contreras M A, Mansfield L M, Egaas B, Li J, Romero M, Noufi R, Rudiger-Voigt E and Mannstadt W 2012 Wide bandgap Cu(In,Ga)Se$_2$ solar cells with improved energy conversion efficiency *Prog. Photovolt., Res. Appl.* **20** 843–50

[22] Keller J, Pearson P, Shariati Nilsson N, Stolt O, Stolt L and Edoff M 2021 Performance limitations of wide-gap (Ag,Cu)(In,Ga)Se$_2$ thin-film solar cells *Sol. RRL* **5** 2100403

[23] Zahedi-Azad S, Maiberg M and Scheer R 2020 Effect of Na-PDT and KF-PDT on the photovoltaic performance of wide bandgap Cu (In,Ga)Se$_2$ solar cells *Prog. Photovolt., Res. Appl.* **28** 1146–57

[24] Maiberg M, Song C-Y, Morawski M, Neduck F, Kempa H, Damm J, Hariskos D, Witte W and Scheer R 2024 Toward digital twins by one-dimensional simulation of thin-film solar cells: cu(In,Ga)Se$_2$ as an example *Phys. Rev. Appl.* **21** 034051

[25] Russell T C R, Saive R, Augusto A, Bowden S G and Atwater H A 2017 The influence of spectral albedo on bifacial solar cells: a theoretical and experimental study *IEEE J. Photovoltaics* **7** 1611–8

[26] Lundberg O, Bodegård M, Malmström J and Stolt L 2003 Influence of the Cu(In,Ga)Se$_2$ thickness and Ga grading on solar cell performance *Prog. Photovolt.* **11** 77–88

[27] Prathapani S, Gharabeiki S, Lauche J, Schwiddessen R, Reyes-Figueroa P, Weinberger N, Melchiorre M, Schlatmann R, Lauermann I and Kaufmann C A 2025 Impact of minimal silver incorporation on chalcopyrite absorbers—origins for improved open-circuit voltages in (Ag,Cu)(In,Ga)Se$_2$ solar cells *Sol. RRL* **9** 2400863